

PAPER

Design and mechanical properties of Mo-10Si-7B alloys doped with lanthanum oxide by a hot pressing process

To cite this article: Wenhui Li *et al* 2019 *Mater. Res. Express* **6** 096593

View the [article online](#) for updates and enhancements.



IOP | ebooks™

Bringing you innovative digital publishing with leading voices to create your essential collection of books in STEM research.

Start exploring the **collection** - download the first chapter of every title for free.

Materials Research Express



PAPER

Design and mechanical properties of Mo-10Si-7B alloys doped with lanthanum oxide by a hot pressing process

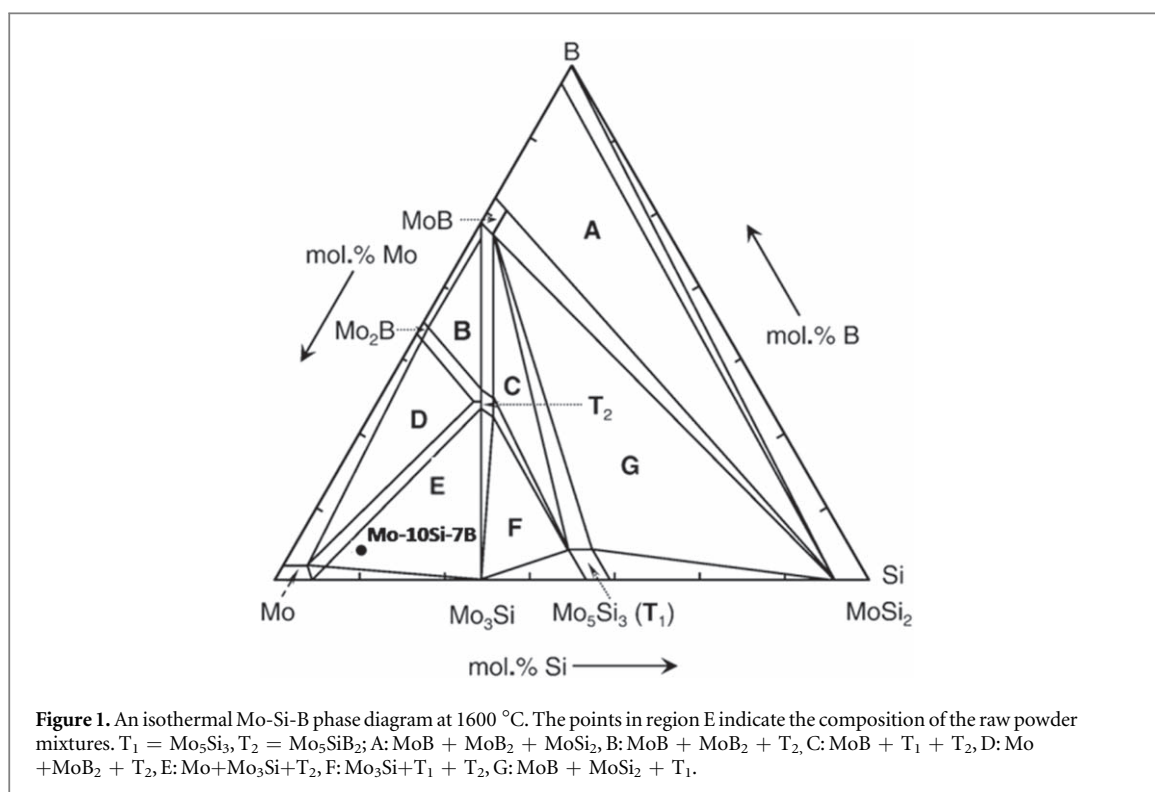
Wenhu Li^{1,2} , Guojun Zhang¹, Taotao Ai², Bin Li¹ and Rui Li¹¹ School of Materials Science & Engineering, Xi'an University of Technology, Xi'an 710048, People's Republic of China² School of Materials Science & Engineering, Shaanxi University of Technology, Hanzhong 723000, People's Republic of ChinaE-mail: zhangguojun@xaut.edu.cn**Keywords:** Mo-Si-B alloys, lanthanum oxide, mechanical alloying, improved bending properties, greater fracture resistance**Abstract**

Mo-10Si-7B alloys doped with different mass fractions (0.3, 0.6, 0.9, and 1.2 wt%) of lanthanum oxide (La_2O_3) were prepared by liquid-liquid doping, mechanical alloying, and hot pressing. The obtained alloys have shown a fine-grained structure comprising of α -Mo, Mo_5SiB_2 , and Mo_3Si phases. The microstructures of the Mo-10Si-7B alloys revealed that their grains became finer with an increase in the content of La_2O_3 . The maximum bending strength of Mo-10Si-7B alloys (1.48 GPa) was obtained upon doping with 0.9 wt% La_2O_3 . The fracture toughness of the corresponding alloys was $\sim 15.58 \text{ MPa}\cdot\text{m}^{1/2}$, indicating that La_2O_3 through liquid-liquid doping significantly improved the bending strength and fracture toughness of doped alloys compared to un-doped alloys. Also, the densities of the obtained alloys were relatively high, mainly due to hot pressing, which reduces the porosity, micro-cracks, and other defects.

1. Introduction

Refractory metal-intermetallic composites consisting of refractory metal solid-solution phase reinforced with intermetallic phases have been identified as potential candidates for applications in power and aerospace industries [1, 2]. Among these materials, Mo-Si-B alloys have gained particular attention as they consist of a molybdenum solid-solution (α -Mo) matrix, three types of silicides, viz. MoSi_2 , Mo_3Si , and Mo_5Si_3 in the Mo-Si system, binary borides including Mo_2B and MoB in the Mo-B system, and a Mo_5SiB_2 ternary boride phase which is uniformly distributed throughout the microstructure. These alloys exhibit excellent mechanical and oxidation properties at temperatures above 1100 °C [3, 4]. The Mo_5SiB_2 and Mo_5Si_3 phases are designated as T_2 and T_1 phases, respectively. Relative to MoSi_2 compounds, Mo_5Si_3 and Mo_3Si exhibit significantly inferior oxidation resistances [5, 6], as the ratio of Mo/Si is less in both Mo_5Si_3 and Mo_3Si compared to MoSi_2 . Recent studies have indicated that B-doping of Mo-Si system effectively improves the oxidation resistance due to the formation of the T_2 phase. However, doping with boride introduces a problem where MoB and Mo_2B compounds are synthesized via an *in situ* reaction in the Mo-rich region. Relative to Mo solid solution, both MoB and Mo_2B compounds exhibit a lower fracture toughness. Figure 1 shows the equilibrium diagram of Mo-Si-B close to Mo-rich region in an isothermal section at 1600 °C. The main phases are α -Mo, Mo_3Si , Mo_5Si_3 , MoSi_2 , MoB , Mo_2B , and Mo_5SiB_2 , which yield about eight triangular phase regions [7–9]. Among these, studies into Mo-Si-B alloys have mainly concentrated on three phase areas of α -Mo+ Mo_3Si + T_2 , α -Mo+ T_2 + Mo_2B , and Mo_3Si + T_1 + T_2 [10–12] and different compositions of Mo-Si-B alloys are found to exhibit different properties. The first two compositions exhibit greater toughness because of the existence of α -Mo phase, which produces greater toughness at room temperature [13]. The final type exhibits excellent resistance to high-temperature oxidation but poor room temperature toughness [11].

However, despite these potential advantages, Mo-Si-B alloys are difficult to employ in practical applications, such as in the turbine blades of the engine, the turbine disk, the combustion chamber, etc [14], as they have insufficient fracture toughness at room temperature. Therefore, in many of the investigations, controlling the microstructure and the addition of other elements in the α -Mo matrix phase are conducted as an effective way to



improve the fracture toughness. Sung-Tag Oh prepared Mo-Si-B intermetallic compounds with a continuous α -Mo matrix by the pulverization of ingot and the reduction of MoO_3 powders using hydrogen [15]. In the studies of Young Do Kim, niobium was added to Mo-Si-B alloy by a powder metallurgical method to improve the mechanical properties, and the fracture toughness of Mo-Nb-Si-B alloy was about $14.5 \text{ MPa}\cdot\text{m}^{1/2}$ [16]. Nan Lin investigated the effects of the content of lanthanum on the microstructure and properties of molybdenum alloy by using a solid-liquid doping method [17]. Hu fabricated $\text{La}(\text{NO}_3)_3$ and La_2O_3 doped TZM alloys by using a powder metallurgy method, and the $\text{La}(\text{NO}_3)_3$ doping method increased the ultimate strength of TZM alloy by 11.2%. Besides, the formation of secondary phases in lanthanum-doped titanium-zirconium-molybdenum alloy was discussed [18, 19].

While many studies have addressed the microstructure and mechanical properties of Mo-Si-B alloys with different contents of doped silicon and boron [20–23], little is known about the effects of the proportion of different components on the microstructure and mechanical properties. The Mo-10Si-7B ternary alloy is a promising candidate which falls in the phase region of α -Mo + $\text{Mo}_3\text{Si} + T_2$. The Mo solid-solution phase accounts for $\sim 50\%$ by volume, which is approximately equal to the sum of the other two phases for Mo-10Si-7B ternary alloy. Studying the microstructure and properties of Mo-10Si-7B ternary alloy can provide us a better understanding of the evolution of microstructure and its influence on the properties of Mo-Si-B alloys. Moreover, Mo-10Si-7B ternary alloys possess an excellent combination of properties suitable for high-temperature applications.

Recently, it has been reported that the addition of rare-earth oxides to Mo-Si-B alloys results into a substantial improvement in the alloy's oxide dispersion-strengthening and resistance to high-temperature oxidation, which affords superior strength and recrystallization temperature characteristics of the alloy compared to their pristine counterparts. Sun designed and manufactured oxide-dispersion-strengthened molybdenum alloys with hierarchical microstructures [24] via a liquid-liquid doping (L-L) process that enabled the control of the grain and its dispersion in a nano-structured regime.

Although there have been many studies on pure Mo and Mo-Si-B alloys doped with rare-earth oxides, little is known about Mo-10Si-7B alloys doped with La_2O_3 by L-L process. In this study, L-L, mechanical alloying, and hot pressing were used to prepare Mo-10Si-7B alloys doped with different mass fractions of La_2O_3 . The effects of La_2O_3 doping by the L-L method on the mechanical properties of Mo-10Si-7B alloys were determined.

2. Experimental procedure

In the experiments of L-L doping, La_2O_3 was first dissolved in an aqueous nitrate solution ($\text{La}(\text{NO}_3)_3$), and then mixed with ammonium tetramolybdate solution ($(\text{NH}_4)_2\text{Mo}_4\text{O}_{13}$). The pH was maintained at 8–9 throughout

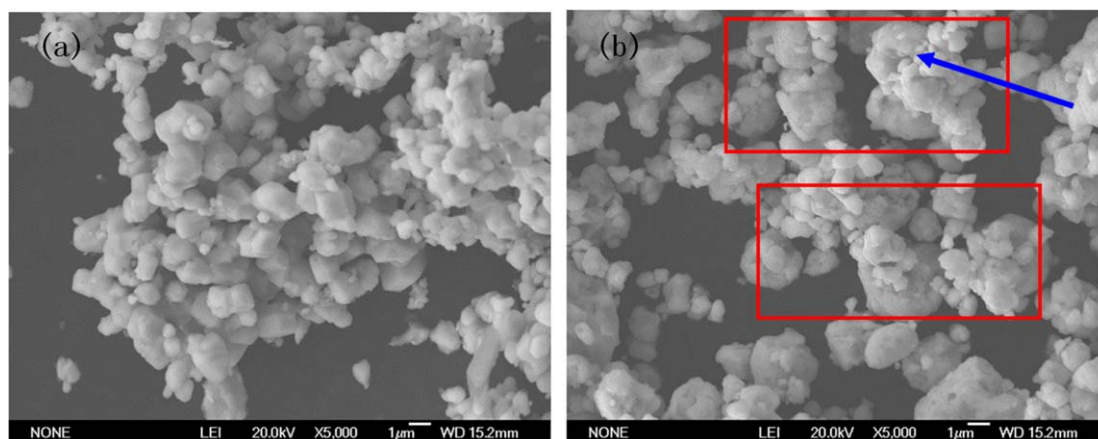
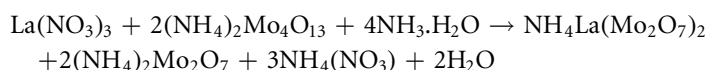


Figure 2. Morphologies of the powders with the composition of Mo-10Si-7B (a) mixed powders (b) mechanical alloying for 15 h.

the experiments. The overall chemical reaction is represented as follows.



This reaction was initiated with the precipitation of $\text{NH}_4\text{La}(\text{Mo}_2\text{O}_7)_2$. Subsequently, $(\text{NH}_4)_2\text{Mo}_2\text{O}_7$ was induced to heterogeneously nucleate on $\text{NH}_4\text{La}(\text{Mo}_2\text{O}_7)_2$, forming a core-shell structure. These mixed powders were then heated to 450 °C for 1 h and then decomposed to form molybdenum oxide enclosing La_2O_3 , and were then immediately reduced to Mo powders in dry H_2 , with embedded La_2O_3 .

Mo- La_2O_3 powders (purity = 99.8 wt%, size $\approx 2.8 \mu\text{m}$, La_2O_3 content = 0.3%–1.2%) were prepared in the laboratory, together with the commercially available Si (99.99 %, size $< 3 \mu\text{m}$) and B (99.99 %, size $< 5 \mu\text{m}$), which were used as raw materials. The Mo-10Si-7B-x La_2O_3 (at%) (x = 0.3, 0.6, 0.9, and 1.2 wt%) alloys were produced using mechanical alloying and hot pressing.

In mechanical alloying, first, Mo- La_2O_3 , Si, and B powders were mixed in a planetary ball-mill with polyurethane balls using a ball-to-powder weight ratio of 1:1 for 24 h at a milling speed of 150 rpm. Following this, the mixed powders were placed in a Retsch PM 400 apparatus at room temperature under Ar atmosphere. The milling media consisted of five 20 mm balls and twenty-seven 10 mm balls confined in a 250 ml vial. Both the balls and vial were fabricated from tungsten carbide. The ball-to-powder weight ratio and the milling speed were 10:1, and 250 rpm, respectively. The mass of total powder was 50 g. Figures 2(a) and (b) exhibit the powder morphologies before and after mechanical alloying using scanning electron microscopy (SEM). These images show that the particles are more spherical, and their boundary is clear, but the agglomeration is more severe before mechanical alloying.

The mixed powders show a typical microstructure with complete homogenization, smaller particle size, less sphericity, agglomeration, and cold welding, after mechanical alloying. There is deformation in the shape of the particles, and the Mo powder is compressed into a sheet by the high-speed collision and impact (as shown in the box), and the powder particles with a relatively strong brittleness such as Si and B are crushed into a granular form (as shown by the arrow). These mechanically alloyed powders were annealed in vacuum under a pressure of 1×10^{-3} Pa and at 1200 °C for 1 h. Following this, the powders were hot-pressed at 50 MPa and sintered in vacuum at 1600 °C for 2 h.

The bending strength and fracture toughness of the sintered compacts were measured to evaluate the mechanical properties. The bending strength was measured in a universal material testing machine (Instron 1185) with a 20 mm span at a crosshead speed of 0.5 mm min^{-1} , while the fracture toughness was tested in the same machine with a 20 mm span at a crosshead speed of 0.05 mm min^{-1} . The transverse rupture strength tests employed specimens with a cross-girder configuration measuring $3 \text{ mm} \times 4 \text{ mm} \times 26 \text{ mm}$. The fracture toughness specimens were of the same dimensions but had a notch with a depth of 2 mm. The fracture toughness values were determined from an energy criterion by integrating the load-displacement curves. Assuming that the material to be linearly elastic, the fracture energy can also be expressed in terms of the stress intensity by $K_{\text{q}} = (G \cdot E')^{1/2}$, where $E' = E/(1 - \nu^2)$ is the plane strain Young's modulus, and ν is the Poisson's ratio ($E = 327 \text{ GPa}$ and $\nu = 0.29$) [25]. The densities of the samples were measured using the Archimedes technique. All reported values are the averages of at least three measurements.

Macroscopic and microscopic photographs of the fracture surfaces of the specimens were obtained using scanning electron microscopy (JSM-6700F). The microstructure of the alloy was also observed using

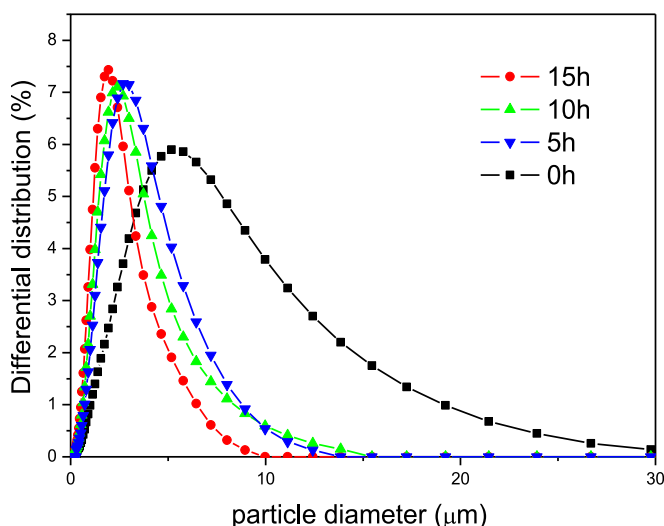


Figure 3. The particle size distribution of the ball-milled and mechanically alloyed powders for 5, 10, and 15 h.

transmission electron microscopy (JEM-3010). Phase identification of the samples was performed by x-ray diffraction (XRD-7000S) using Cu-K α radiation source and a step size of 0.05°.

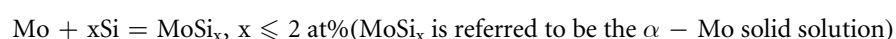
3. Results and discussion

3.1. Phase composition and microstructure

The particle size distribution of the powders which were ball-milled and mechanically alloyed for 5, 10, and 15 h are shown in figure 3. The grain size of the powder milled for 24 h was $\sim 5.182 \mu\text{m}$. After 5, 10, and 15 h of mechanical alloying, the particle size decreased from 5.182 to 2.690, 2.412, and 1.938 μm , respectively, and the particle size of all the powders exhibited a normal distribution. After mechanical alloying, the median diameter (D50) of the powders was significantly reduced, and the particle size distribution became narrower, implying that the particle size becomes more uniform as the alloy powders are refined. Compared to the study of He [26], the obtained MA powder has a wider particle size distribution and smaller median size. This is consistent with the SEM images and implies that mechanical alloying is applicable for grinding powders, leading to an increased surface energy of the powders and accelerating the sintering process [20, 21].

Figure 4 shows the XRD diffraction patterns of Mo-10Si-7B-1.2La₂O₃ powders after ball milling, 15 h of mechanical alloying and subjected to annealing treatment at 1200°C. It can be seen from figure 4 that there is only a diffraction peak of Mo, and no diffraction peaks for Si, B, and La₂O₃ after mixing could be noted. The main reason is due to that the contents of Si, B, and La₂O₃ are lower than Mo. It was found that, after mechanical alloying, the width of the XRD diffraction peak of the mixture increased and the peak strength decreased as compared to the diffraction peak before alloying. The crystallinity of the powder particles becomes worse with an absolute deviation to the right angle. After annealing treatment of mechanically alloyed powder, it is found from XRD that the intensity of the diffraction peak increases and the width of the diffraction peak becomes narrower. These results show that the amorphous intermetallic phase produced by mechanical alloying begins to crystallize at high temperature.

Figure 5 depicts the XRD patterns of the hot-pressed specimens with doped La₂O₃ contents of 0.3, 0.6, 0.9, and 1.2 wt%. It is evident that the four diffraction patterns are almost identical, and all the exhibited peaks are attributed to the expected reaction products of Mo₃Si, Mo₅SiB₂, and α -Mo solid solution phases. In case of an α -Mo solid solution, relatively small solute atoms of Si occupy interstitial positions between the crystal lattice of molybdenum, which acts as the solvent. This indicates that neither the La₂O₃ content nor the doping method affects the phase composition. Also, the diffraction peak intensity of α -Mo is higher compared to the other two phases, corresponding to the isothermal section of Mo-Si-B equilibrium phase diagram close to the Mo-rich region at 1600 °C. Therefore, the following reactions may occur [27, 28]:



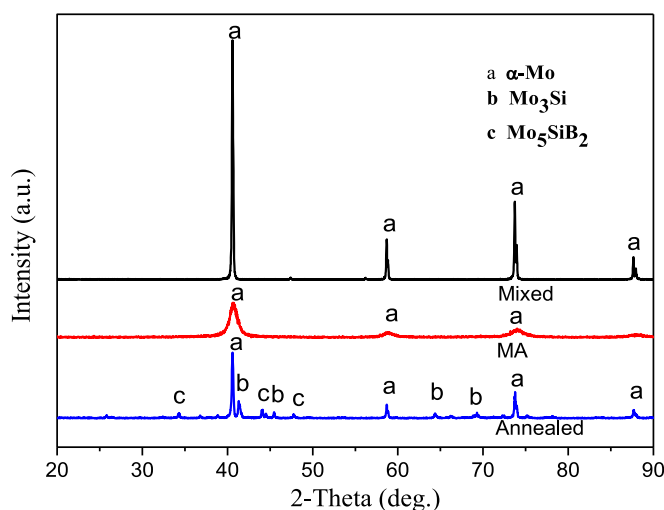


Figure 4. XRD curves of Mo-10Si-7B-1.2La₂O₃ powders after milling, 15 h of mechanical alloying and annealing.

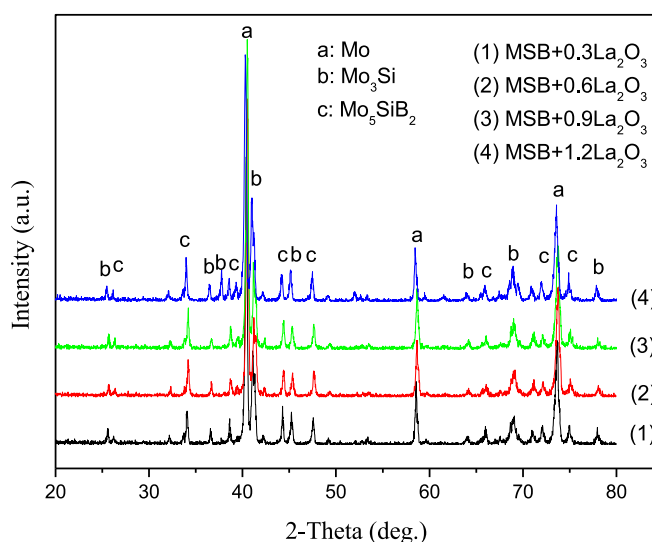
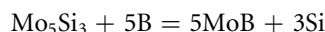
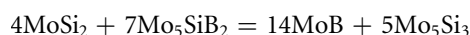
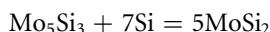
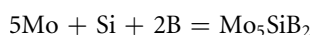
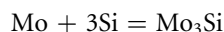


Figure 5. XRD patterns of Mo-10Si-7B alloys with different mass fractions of La₂O₃.



In SEM measurements, the microstructures of hot-pressed specimens were observed using backscattered electrons (figure 6). The bright-white grains and the gray/grayish-white phases which were identified by XRD and TEM to be the α -Mo phase (the solid arrows as highlighted in figure 6(a)), and the Mo₅SiB₂ (indicated by arrow in figure 6(b)) and Mo₃Si phases (indicated by arrow in figure 6(c)), respectively. The grayish-black spherical phases, several hundred nanometers in size, are distributed in the grain boundary of La₂O₃. The black spherical holes (indicated by an arrow in figure 6(d)) are the sintered holes that are smaller in size. The grain size is affected by the La₂O₃ content.

Figure 7 shows the microstructure and crystal particle size of the alloys both with and without La₂O₃ doping. The addition of La₂O₃ significantly decreased the grain size of the Mo-Si-B alloys, thereby preventing the movement of grain boundary and restraining the growth of grain in the same sintering process. It was previously reported that the growth of Mo₅SiB₂ and Mo₃Si grains was controlled by the movement of grain boundary

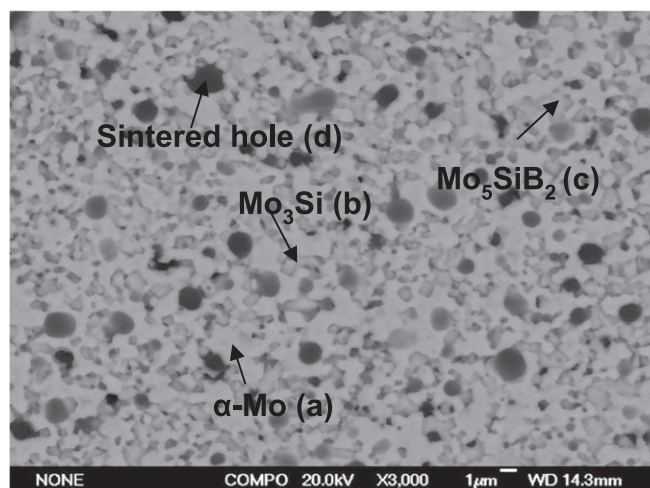


Figure 6. SEM images of Mo-10Si-7B-0.9La₂O₃ alloys.

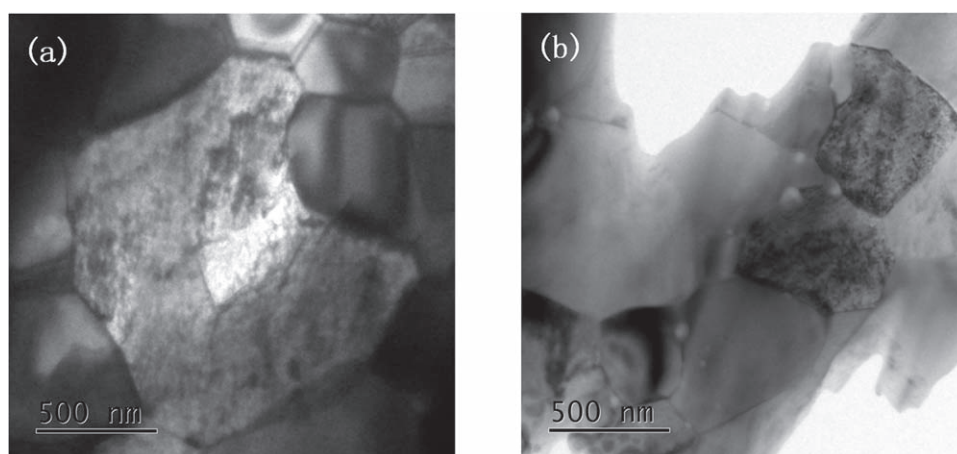


Figure 7. The microstructural morphologies of the alloys using TEM (a) without the addition of La₂O₃ (b) with the addition of La₂O₃.

[29–31]. The Mo₅SiB₂ and Mo₃Si grains become finer with an increase in the content of La₂O₃. Therefore, it can be deduced that La₂O₃ doping inhibits the growth of Mo₅SiB₂ and Mo₃Si grains.

3.2. Mechanical properties

3.2.1. Bending strength at room temperature

The room-temperature strength of the hot-pressed Mo-10Si-7B alloys is shown in figure 8. The bending behaviors are similar for the doped and un-doped Mo-10Si-7B alloys. Both the bending strength and breaking strain of the doped alloys increase with an increase in the content of La₂O₃.

The bending strength of Mo-10Si-7B alloys is remarkably improved with an increase in the content of La₂O₃ from 0.3 to 0.9 wt%, and decreased when the La₂O₃ content reached 1.2 wt%. A quantitative comparison reveals that the bending strength of Mo-10Si-7B alloy is 1.06 GPa, while for Mo-10Si-7B + (0.3, 0.6, 0.9, 1.2 wt%) La₂O₃ alloys are 1.33, 1.44, 1.48, and 1.18 GPa, respectively. In terms of microstructure characteristics, the fine grain and dispersion strengthening mechanisms are most likely responsible for the enhanced strength.

The stress-deflection curves of the alloy (figure 8) exhibited only a linear elastic stage but without any yield stage. In the elastic stage, the highest point is the one at which the sample breaks via a typical brittle fracture. In comparison, the bending strength of 0.9 wt% La₂O₃-doped Mo-10Si-7B alloy (1.48 GPa) is the highest among La₂O₃-doped alloys. Here, the strengthening effect of La₂O₃ on the alloy is evident.

Figures 9(a)–(d) show the SEM macroscopic images of the fracture surfaces of Mo-10Si-7B doped with 0.3, 0.6, 0.9, and 1.2 wt% La₂O₃, respectively, which were obtained in the bending strength test at room temperature.

Figure 9 shows that the cracks are formed rapidly after an unstable expansion, and the fracture mode is a brittle fracture. The fracture is undulating, and there are river-like tear edges after the fracture. The cracks

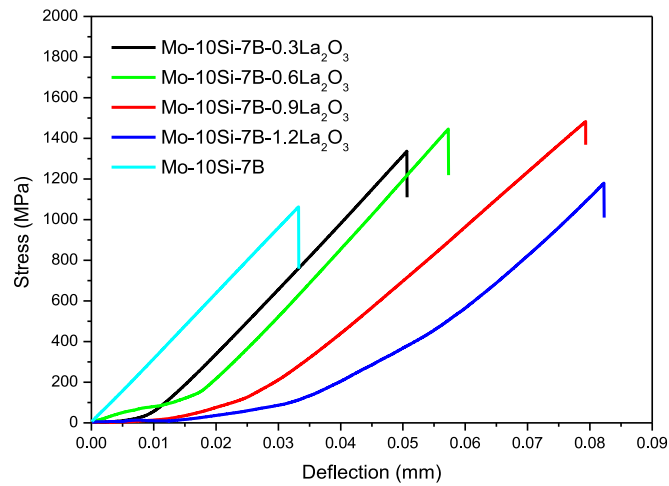


Figure 8. The stress-deflection curves of different mass fractions of La_2O_3 doped Mo-10Si-7B alloys obtained through room temperature bending test.

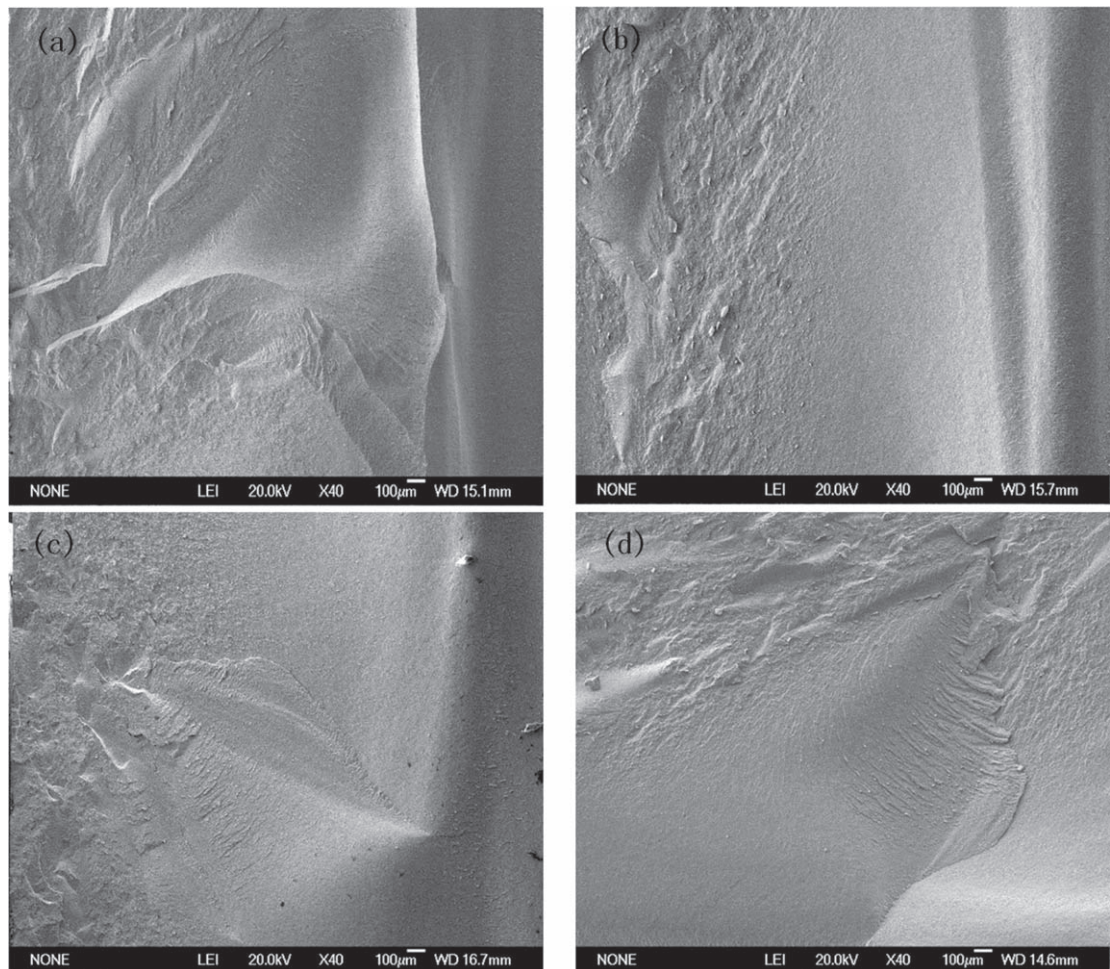


Figure 9. SEM macroscopic images of the alloys obtained through room temperature bending test: (a) Mo-10Si-7B + $0.3\text{La}_2\text{O}_3$ (b) Mo-10Si-7B + $0.6\text{La}_2\text{O}_3$ (c) Mo-10Si-7B + $0.9\text{La}_2\text{O}_3$ (d) Mo-10Si-7B + $1.2\text{La}_2\text{O}_3$.

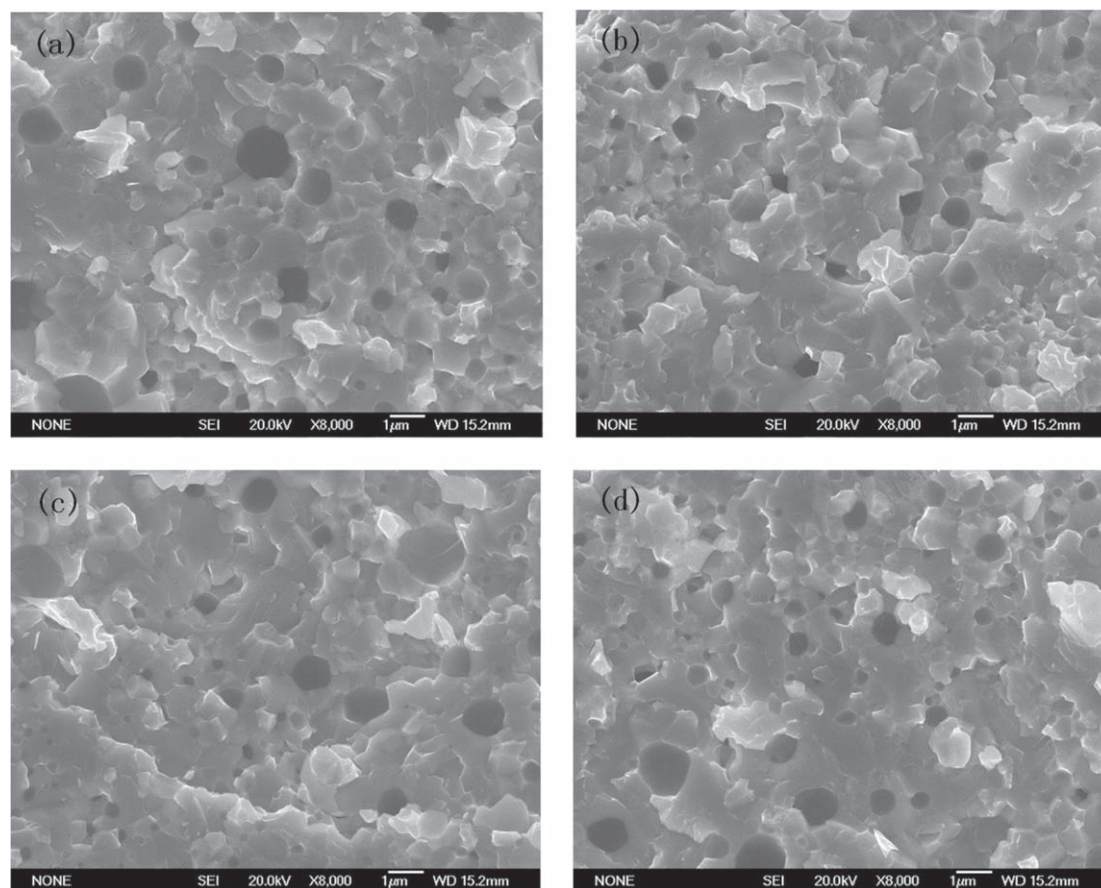


Figure 10. SEM microscopic images of the alloys obtained through room temperature bending test: (a) Mo-10Si-7B + 0.3La₂O₃ (b) Mo-10Si-7B + 0.6La₂O₃ (c) Mo-10Si-7B + 0.9La₂O₃ (d) Mo-10Si-7B + 1.2La₂O₃.

Table 1. The fracture toughness and density of Mo-10Si-7B alloys with different mass fractions of La₂O₃.

| Materials | Mo-10Si-7B | Mo-10Si-7B-0.3 La ₂ O ₃ | Mo-10Si-7B-0.6 La ₂ O ₃ | Mo-10Si-7B-0.9 La ₂ O ₃ | Mo-10Si-7B-1.2 La ₂ O ₃ |
|--|------------|--|--|--|--|
| Fracture toughness (MPa m ^{1/2}) | 13.35 | 14.51 | 14.66 | 15.58 | 15.20 |
| Density (g cm ⁻³) | 8.960 | 8.925 | 8.998 | 8.971 | 8.896 |

propagate in many different directions and the formation region of crack is in the front of the crack, from which the crack grows back.

Figures 10(a)–(d) show the SEM microscopic images of the fracture surfaces of Mo-10Si-7B doped with 0.3, 0.6, 0.9, and 1.2 wt% La₂O₃ alloy, respectively, which were obtained in the bending-strength test at room temperature.

The mode of fracture of the alloy shows brittle cleavage fracture, but the fracture morphologies of the alloys with different La₂O₃ contents are not apparent. At the micro scale, the fracture mode of the alloy includes transcrystalline, intercrystalline, and mixed fractures of trans-grain and inter-grain, which is characteristic of Mo-Si-B alloy [9]. There are also some protruding grains and holes produced as a result of the hard Mo₃Si and Mo₅SiB₂ particles being pulled out of the α-Mo phase.

The La₂O₃ particles are mainly distributed on the interface between the α-Mo phases and intermetallic phases, which could hinder the expansion of cracks, promote the deflection of cracks, and increase the crack propagation paths, contributing to the improvement in the strength of the alloys.

3.2.2. Fracture toughness

The experimentally determined fracture toughness and density of the alloys are listed in table 1. At room temperature, K_q of Mo-10Si-7B alloy is 13.35 MPa m^{1/2}, which is lower than that of Mo-10Si-7B alloys with different mass fractions of doped La₂O₃. The SEM micrographs of the room-temperature fracture surfaces are

shown in figures 9 and 10, which demonstrate apparent cleavage facets and a river pattern. Also, they reveal that the principal failure mechanism is a mixed-mode fracture. Some particle pull-outs are also observed in the fracture surface.

An increase could be due to two main reasons: fine-grain toughening and particle toughening. Material toughness can be effectively improved by refining the grains. However, this refinement of grain increases the per-unit-volume of the grain boundary area. When the deformation moves from one grain to an adjacent grain across the grain boundary, the resistance of the dislocation and the difficulty of crack generation increases, thereby increasing the energy consumption. Consequently, increasing the grain boundary area improves its blocking of crack expansion.

On the other hand, La_2O_3 -doped Mo powder was prepared using the L-L doping technique. In this doping, many of the formed core-shell structures are thermodynamically stable and substantially increase the number of Mo nuclei in the subsequent reactions. Ultrafine Mo grains and optimized La_2O_3 particles are the most important microstructural features of the L-L doping-derived Mo-Si-B alloys. Furthermore, La_2O_3 particles distributed in the α -Mo matrix present an obstacle to the dislocation, thus promoting a dislocation pile-up. Due to the hardness of La_2O_3 particles, the dislocation cannot break the La_2O_3 particles, and must instead move around them. Therefore, the L-L-doped La_2O_3 particles have a second-phase dispersion strengthening effect, which increases the bending strength and toughness.

The densities of the alloys are relatively high, which may be mainly due to the hot pressing that reduces the porosity, micro-cracks, and other defects, but increases the density of the sintered alloy. This also increases the fracture toughness of Mo-Si-B alloy.

However, when the La_2O_3 content reaches 0.9%, the fracture toughness of the material decreased. This is mainly due to the produced microcracks at the grain boundaries and because of an increase in the intergranular cracking with an increase in the content of second-phase particles at the grain boundary. An increase in the amount of precipitates in the grain boundaries, and micro-cracks as well as the possibility of increasing the sinter in various defects and pores caused by the sintering process decreased.

The fracture toughness of the alloy does not increase with an increase in the content of lanthanum oxide, which is mainly due to that, on the one hand, a difference in the grain size of the alloys with different lanthanum oxide content is not very obvious (figure 10). On the other hand, Mo-10Si-7B alloy is brittle at room temperature and the alloy has relatively a tough α -Mo phase, but the volume fraction of α -Mo phase is only about 50% of the alloy. However, an α -Mo solid solution was formed by the solid solution of Si into Mo, which decreased the toughness of Mo although the strength was increased. The lack of plasticity of α -Mo phase resulted in the weakening of crack trapping ability. The contact stress between intermetallic phases cannot be effectively released by the plastic deformation of α -Mo phase.

4. Conclusions

- (1) La_2O_3 -doped Mo-10Si-7B alloys are composed of α -Mo, Mo_3Si , and Mo_5SiB_2 phases. The intermetallic Mo_3Si and Mo_5SiB_2 phases are distributed over a continuous α -Mo matrix. When the alloys are doped with La_2O_3 , the grain sizes and intermetallic particle sizes of the alloys become refined and distributed more homogeneously.
- (2) The bending strength of Mo-10Si-7B alloys doped with 0.9 wt% La_2O_3 using L-L doping method improved to 1.48 GPa. Also, the bending strength was continuously increased when the amount of La_2O_3 doping was increased from 0.3 to 0.9 wt%, after which it decreased; in this case, the bending strength was mainly affected by the presence of fine grains and increased particle dispersion.
- (3) The mode of fracture of the alloy is brittle cleavage fracture. The L-L doping method improved the fracture toughness of the doped Mo-10Si-7B alloys. At room temperature, K_{q} of the Mo-10Si-7B alloy is $13.35 \text{ MPa m}^{1/2}$, which is lower than that of Mo-10Si-7B alloys with different mass fractions of La_2O_3 . The primary toughening mechanisms are those of the fine grains and particles.

Acknowledgments

This study was supported by the National Natural Science Foundation of China (Grant Nos. 51602186, 51671116, and 51674196) and the Key Project of Natural Science Basic Research Plan in Shaanxi Province of China (Program No. 2016JZ016).

ORCID iDs

Wenhu Li  <https://orcid.org/0000-0002-7795-5003>

References

- [1] Jéhanno P, Heilmaier M, Kestler H, Boning M, Venskutonis A, Bewlay B and Jackson M 2005 Assessment of a powder metallurgical processing route for refractory metal silicide alloys *Metall. Mater. Trans A* **36** 515–23
- [2] Perepezko J H 2009 The hotter the engine, the better *Science* **326** 1068–9
- [3] Levashov E A, Pogozhev Y S, Potanin A Y, Kochetov N A, Kovalev D Y, Shvyndina N V and Sviridova T A 2014 Self-propagating high-temperature synthesis of advanced ceramics in the Mo–Si–B system: kinetics and mechanism of combustion and structure formation *Ceram. Int.* **40** 6541–52
- [4] Das J, Roy B, Kumar N K and Mitra R 2017 High temperature oxidation response of Al/Ce doped Mo–Si–B composites *Intermetallics* **83** 101–9
- [5] Yamauchi A, Yoshimi K, Kurokawa K and Hanada S 2007 Synthesis of Mo–Si–B in situ composites by mechanical alloying *J. Alloy. Compd.* **434–435** 420–3
- [6] Sakidja R, Myers J, Kim S and Perepezko J H 2000 The effect of refractory metal substitution on the stability of Mo(ss) + T2 two-phase field in the Mo–Si–B system *Int. J. Refract. Met. Hard Mater.* **18** 193–204
- [7] Byun J M, Hwang S H, Lee S, Suk M J, Oh S T and Kim Y D 2015 Microstructure control of Mo–Si–B alloy for formation of continuous α -Mo phase *Int. J. Refract. Met. Hard Mater.* **53** 61–5
- [8] Kruger M, Franz S, Saage H, Heilmaier M, Schneibel J H, Jéhanno P, Boning M and Kestler H 2008 Mechanically alloyed Mo–Si–B alloys with a continuous α -Mo matrix and improved mechanical properties *Intermetallics* **16** 933–41
- [9] Schneibel J H, Kramer M J and Easton D S 2002 A Mo–Si–B intermetallic alloy with a continuous α -Mo matrix *Scripta Mater.* **46** 217–21
- [10] Rioult F A, Imhoff S D, Sakidja R and Perepezko J H 2009 Transient oxidation of Mo–Si–B alloys: effect of the microstructure size scale *Acta Mater.* **57** 4600–13
- [11] Zhang G J, He W, Li B, Zha Y and Sun J 2013 Effect of Si/B ratio on the microstructure and mechanical properties of lanthanum oxide-doped Mo–Si–B alloys *J. Alloy. Compd.* **577** 217–21
- [12] Schneibel J H and Sekhar J A 2003 Microstructure and properties of MoSi₂–MoB and MoSi₂–Mo₅Si₃ molybdenum silicides *Mat. Sci. Eng. A* **340** 204–11
- [13] Lemberg J A, Middlemas M R, Weingärtner T, Gludovatz B, Cochran J K and Ritchie R O 2012 On the fracture toughness of fine-grained Mo–3Si–1B (wt%) alloys at ambient to elevated (1300 °C) temperatures *Intermetallics* **20** 141–54
- [14] Jain P and Kuma K S 2010 Dissolved Si in Mo and its effects on the properties of Mo–Si–B alloys *Scripta Mater.* **62** 1–4
- [15] Kwon N Y et al 2017 Synthesis of Mo–Si–B intermetallic compounds with continuous α -Mo matrix by pulverization of ingot and hydrogen reduction of MoO₃ powders *Int. J. Refract. Met. Hard Mater.* **65** 25–8
- [16] Byun J M et al 2017 Mechanical properties of Mo–Nb–Si–B quaternary alloy fabricated by powder metallurgical method *Int. J. Refract. Met. Hard Mater.* **65** 14–8
- [17] Yang X Q et al 2016 Effects of the lanthanum content on the microstructure and properties of the molybdenum alloy *Int. J. Refract. Met. Hard Mater.* **61** 179–84
- [18] Hu P et al 2017 High temperature mechanical properties of TZM alloys under different lanthanum doping treatments *J. Alloy. Compd.* **711** 64–70
- [19] Hu B L et al 2018 Secondary phases formation in lanthanum-doped titanium-zirconium-molybdenum alloy *J. Alloy. Compd.* **757** 340–7
- [20] Abbasi A R and Shamanian M 2011 Synthesis of Mo₅SiB₂ based nanocomposites by mechanical alloying and subsequent heat treatment *Mat. Sci. Eng. A* **528** 3295–301
- [21] Abbasi A R and Shamanian M 2011 Synthesis of α -Mo–Mo₅SiB₂–Mo₃Si nanocomposite powders by two-step mechanical alloying and subsequent heat treatment *J. Alloy. Compd.* **509** 8097–104
- [22] Schneibel J H, Liu C T, Easton D S and Carmichael C A 1999 Microstructure and mechanical properties of Mo–Mo₃Si–Mo₅SiB₂ silicides *Mat. Sci. Eng. A* **261** 78–83
- [23] Parthasarathy T A, Mendiratta M G and Dimiduk D M 2002 Oxidation mechanisms in Mo reinforced Mo₅SiB₂(T2)–Mo₃Si alloys *Acta Mater.* **50** 1857–68
- [24] Liu G, Zhang G J, Jiang F, Ding X D, Sun Y J, Sun J and Ma E 2013 Nanostructured high-strength molybdenum alloys with unprecedented tensile ductility *Nat. Mater.* **12** 344–50
- [25] Schneibel J H, Kramer M J, Unal O and Wright R N 2001 Processing and mechanical properties of a molybdenum silicide with the composition Mo–12Si–8.5B *Intermetallics* **9** 25–31
- [26] Yang X Q et al 2015 The influences of La doping method on the microstructure and mechanical properties of Mo alloys *Int. J. Refract. Met. Hard Mater.* **51** 301–8
- [27] Kim S and Perepezko J H 2006 Interdiffusion kinetics in the Mo₅SiB₂ (T2) phase *J. Phase. Equilib. Diff.* **27** 605–13
- [28] Hayashi T, Ito K and Numakura H 2005 Reaction diffusion of MoSi₂ and Mo₅SiB₂ *Intermetallics* **13** 93–100
- [29] Zhang G J, Zha Y, Li B, He W and Sun J 2013 Effects of lanthanum oxide content on mechanical properties of mechanical alloying Mo–12Si–8.5B (at%) alloys *Int. J. Refract. Met. Hard Mater.* **41** 585–9
- [30] Zhang G J, Dang Q, Kou H, Wang R H, Liu G and Sun J 2013 Microstructure and mechanical properties of lanthanum oxide-doped Mo–12Si–8.5B(at%) alloys *J. Alloy. Compd.* **577** s493–8
- [31] Zhang G J, Kou H, Dang Q, Liu G and Sun J 2012 Microstructure and oxidation resistance behavior of lanthanum oxide-doped Mo–12Si–8.5B alloys *Int. J. Refract. Met. Hard Mater.* **30** 6–11